ACS APPLIED MATERIALS & INTERFACES

Research Article

www.acsami.org

Well-Defined Nanostructured Surface-Imprinted Polymers for Highly Selective Magnetic Separation of Fluoroquinolones in Human Urine

Yonghuan He, Yanyan Huang,* Yulong Jin, Xiangjun Liu, Guoquan Liu, and Rui Zhao*

Beijing National Laboratory for Molecular Sciences, CAS Key Laboratory of Analytical Chemistry for Living Biosystems, Institute of Chemistry, Chinese Academy of Sciences, Beijing, China

Supporting Information

ABSTRACT: The construction of molecularly imprinted polymers on magnetic nanoparticles gives access to smart materials with dual functions of target recognition and magnetic separation. In this study, the superparamagnetic surface-molecularly imprinted nanoparticles were prepared via surface-initiated reversible addition−fragmentation chain transfer (RAFT) polymerization using ofloxacin (OFX) as template for the separation of fluoroquinolones (FQs). Benefiting from the living/controlled nature of RAFT reaction, distinct core−shell structure was successfully constructed. The highly uniform nanoscale MIP layer was homogeneously grafted on the surface of RAFT agent TTCA modified Fe_3O_4@SiO_2 nanoparticles, which favors the fast mass transfer and rapid binding kinetics. The target binding assays demonstrate the desirable adsorption capacity and imprinting efficiency of Fe_3O_4@MIP. High selectivity of Fe_3O_4@MIP toward FQs (ofloxacin, pefloxacin, enrofloxacin, norfloxacin, and gatifloxacin) was exhibited by competitive binding assay. The Fe_3O_4@MIP nanoparticles were successfully applied for the direct enrichment of five FQs from human urine. The spiked human urine samples were determined and the recoveries ranging from 83.1 to 103.1% were obtained with RSD of 0.8−8.2% (n = 3). This work provides a versatile approach for the fabrication of well-defined MIP on nanomaterials for the analysis of complicated biosystems.

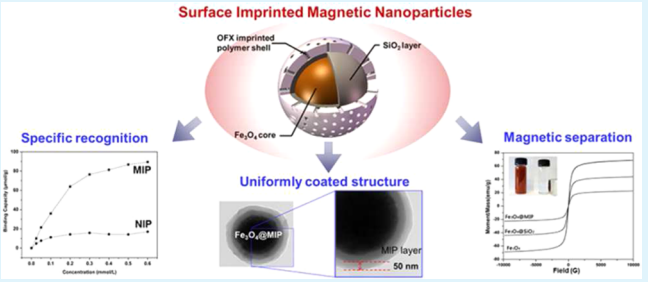

KEYWORDS: *molecularly imprinted polymer, reversible addition−fragmentation chain transfer polymerization, superparamagnetic, core−shell, fluoroquinolones, human urine*

1. INTRODUCTION

Molecularly imprinted polymers (MIPs), featuring high specificity, good stability, ease of preparation, and low cost, are receiving remarkable attention as smart and robust materials for chemical and biochemical analyses.[1,2] With tailor-made binding sites, MIPs not only recognize the size and shape of a given template but also respond to the functional groups of the molecule.[3,4] Successful applications of MIPs have been demonstrated in various fields including chem/biosensors,[5,6] solid phase extraction,[7−10] catalysis,[11,12] and artificial enzyme inhibitor/antibody.[13−15] Even though MIPs are still suffering from the problems, such as incomplete template removal, slow mass transfer, poor site accessibility, irregular shape, or heterogeneous distribution of binding sites, which restrict the wide and deep applications of MIPs.[1] Many efforts have been made to address the above issues.

Thanks to the surface location of the imprinted sites and caves, surface imprinted technique is becoming one of the most effective ways to improve the MIP preparation. Surface-imprinted polymers reveal high binding capacities, fast mass transfer, and rapid binding kinetics due to the easy accessibility to recognition sites and the homogeneous distribution of binding sites.[16,17] Moreover, the MIP materials with magnetic property are superior for easy handling and fast separation since they can be easily collected and isolated by an external magnetic field.[18] In recent years, MIP-functionalized magnetic composites have become a hotspot because of the bifunctional performance of the selectivity for the target molecule and the rapid magnetic response. Lin et al. developed amylase-imprinted magnetic polymers as enzyme carriers for investigating the catalytic processes.[19] Lee et al. fabricated the magnetic MIP nanoparticles for the sensing and extraction of albumin, creatinine and lysozyme in urine sample.[20] Lu et al. prepared the core−shell Fe_3O_4@MIP nanoparticles for selective extraction of environmental contaminant bisphenol A.[21] Because the surface MIP shell is crucial to the template binding property, the construction MIP layers with well-defined, uniform morphology and homogeneously distributed binding sites is still urgently needed.

Controlled/living radical polymerization (CLRP) provides a facile way to grow nanostructured films with controlled composition and functionality.[1] With negligible chain termination and slower rate, CLRP can overcome the defect of the commonly used free radical polymerization where undesired

Received: April 4, 2014
Accepted: May 23, 2014
Published: May 23, 2014

   dx.doi.org/10.1021/am5020666 | ACS Appl. Mater. Interfaces 2014, 6, 9634−9642

chain transfer and termination occur during MIP preparation. Because of these intrinsic advantages, CLRP including atom transfer radical polymerization (ATRP), nitroxide-mediated polymerization (NMP), and reversible addition−fragmentation chain transfer (RAFT), is emerging as an appealing approach for grafting surface imprinted polymers on nanoparticles.[22,23] Among these, RAFT polymerization is an ideal choice not only due to its mild reaction condition, free from the contamination of metal catalysts, but also because it is compatible with the broadest range of monomers and allows postpolymerization modification.[24] Benefiting from its controlled/living property, RAFT polymerization also gives access to the formation of well-defined biocompatible polymer layer on magnetic nanoparticles, and thus significantly facilitates their applications in complex real systems.[25]

Fluoroquinolones (FQs) are a family of synthetic broad-spectrum antibiotic drugs. By inhibiting mRNA transcription and DNA replication, FQs are effective against both Gram-positive and Gram-negative bacteria.[26] However, they are also found to affect mammalian cell replication and associated with a great number of adverse drug reactions, including tendon damage, peripheral neuropathy as well as psychiatric side effect. Moreover, drug resistance has also been detected during FQs usage. For the safety concern, licensed uses of fluoroquinolones is now limited. The European Union has established specific permitted maximum residue limits for fluoroquinolones in foodstuffs of animal origin in order to control illegal usage and exceeding contamination that would affect human health.[27] Therefore, monitoring FQs residues in biological samples and animal products is of great importance. Several MIPs have been prepared for the enrichment and detection of fluoroquinolones.[8,28−31] The application of the merits of RAFT polymerization for the construction of MIPs of any fluoroquinolones has not been reported yet.

In this work, the novel superparamagnetic OFX-imprinted nanoparticles with uniform coating of MIP shell were prepared using surface-initiated RAFT polymerization for the separation of FQs. The Fe_3O_4 nanoparticles were functionalized with a silica layer, which enabled the subsequent anchoring of RAFT agent. The growth of well-defined MIP layer on the surface of silica was accomplished via grafting from approach. The resultant Fe_3O_4@MIP was characterized by transmission electron microscopy (TEM), Fourier-transform infrared spectroscopy (FT-IR), vibrating sample magnetometry (VSM), thermogravimetric analysis (TGA), X-ray photoelectron spectroscopy (XPS) and X-ray diffraction (XRD). The adsorption and separation properties of the bifunctional Fe_3O_4@MIP nanoparticles were further evaluated by equilibrium binding assay, binding capacity and selective experiments. In addition, the practical application of Fe_3O_4@MIP nanoparticles for real biological sample was further assessed by the simultaneous enrichment of five FQs from human urine.

2. EXPERIMENTAL SECTION

2.1. Reagents and Materials. Ferric chloride anhydrous ($FeCl_3$), sodiumacetate anhydrous (NaAC), tirsodium citrate, ethylene glycol, tetraethoxysilane (TEOS), dichloromethane, toluene and ethylene glycol were obtained from Beijing Chemical Works (Beijing, China). Pefloxacin (PEF) and enrofloxacin (ENRO) were purchased from Xi'an Huicheng Biomedicine Co., Ltd. (Xi'an China). Ofloxacin (OFX), norfloxacin (NOR) and gatifloxacin (GAT) were purchased from Taiyuan Kangruibao Veterinary Drug Manufacture Co., Ltd. (Taiyuan, Shanxi, China). Sulfamethoxazole (SMO) was obtained from National Institute for Food and Drug Control (Beijing, China). l,3-aminopropyltriethoxysilane (APTES) and bisphenol A (BPA) were purchased from Aladdin Industrial Corporation (Shanghai, China). *N,N′*-dicyclohexylcarbodiimide (DCC) was purchased from Sinopharm Chemical Reagent Beijing Co., Ltd. (Beijing, China). Acrylic acid (AA), methacrylate acid (MAA), ethylene glycol dimethacrylate (EGDMA), azobis(isobutyronitrile)(AIBN) and tricaprylylmethylammonium chloride were purchased from J&K Scientific Ltd. (Beijing, China). Methanol was obtained from Concord Technology Co., Ltd. (Tianjin, China). Ultrapure water from a Milli-Q water purification system (Millipore, Massachusetts, USA) was used throughout. Toluene was dried through molecular sieve and distilled under reduced pressure. All other reagents are of analytical grade and used without further disposal.

2.2. Synthesis of the RAFT Agent S-1-Dodecyl-S′-(α,α′-dimethyl-α″-aceticacid) Trithiocarbonate (TTCA). The RAFT agent TTCA was synthesized according to the literature.[32] 1-Dodecanethiol (12 mL, 0.05 mol), acetone (30.7 mL, 0.41 mol) and tricaprylylmethylammonium chloride (0.81 g, 0.002 mol) were mixed in a flask and cooled below 10 °C under the protection of N_2 gas flow. After stirring for 10 min, sodium hydroxide solution (3.35 g, 0.042 mol, 50 wt %) was dropwise added into the flask within 20 min. The reaction was going on for additional 15 min. Then, carbon disulfide (2.41 mL, 0.05 mol) dissolved in acetone (5.15 mL, 0.86 mol) was dropwise added within 20 min. Ten minutes later, chloroform (4.80 mL, 0.075 mol) was added followed by the addition of sodium hydroxide solution (16.0 g, 0.25 mol, 50 wt %). The reaction mixture was stirred overnight. Ultrapure water (75 mL) and concentrated HCl (12.5 mL) were orderly added into the flask to acidify the solution. The precipitates were collected and washed with 2-propanol (100 mL). The TTCA solution was concentrated to dryness, and then the residue was recrystallized from hexane to obtain yellow crystalline solid TTCA.

2.3. Preparation of Fe_3O_4@MIP Nanoparticles. *2.3.1. Synthesis of Fe_3O_4@SiO_2 Nanoparticles.* Fe_3O_4 magnetic nanoparticles were synthesized by solvothermal reaction according to the literature.[33] The Fe_3O_4@SiO_2 nanoparticles were synthesized according to the reported method.[34] Briefly, Fe_3O_4 magnetic nanoparticles (0.3 g) were dispersed in a mixed solution of ethanol (160 mL), ultrapure water (40 mL) and concentrated ammonia aqueous solution (5 mL, 25 wt %). The dispersion mixture was sonicated for 15 min, followed by the addition of TEOS (0.7 mL, 3.1 mmol). After stirring at 40 °C for 8 h, the Fe_3O_4@SiO_2 nanoparticles were separated and washed with ethanol and ultrapure water for three times, respectively, and dried under vacuum.

2.3.2. Preparation of Fe_3O_4@SiO_2@NH_2 Nanoparticles. Amine functionalization of Fe_3O_4@SiO_2 nanoparticles was realized by reacting with APTES. Briefly, anhydrous toluene (50 mL) was placed in a flask, in which Fe_3O_4@SiO_2 nanoparticles (0.4 g) were added. The mixture was sonicated for 30 min, followed by the addition of APTES (4 mL). The reaction mixture was stirred at 120 °C for 24 h with N_2 gas protection. The resultant Fe_3O_4@SiO_2@NH_2 nanoparticles were washed with anhydrous toluene and acetone for three times, respectively, and dried under vacuum.

2.3.3. Preparation of Fe_3O_4@MIP and Fe_3O_4@NIP Nanoparticles. Fe_3O_4@SiO_2@NH_2 nanoparticles (0.3 g) were dispersed in anhydrous DMF (30 mL). The mixture was sonicated for 15 min and ice-cooled, followed by the addition of TTCA (0.73 g, 2 mmol) and DCC (0.43 g, 2 mmol). The mixture was stirred at 0 °C for 2 h and then at room temperature for 12 h. The TTCA-grafted nanoparticles were collected by a magnet, washed with DMF and methanol three times respectively, and dried under a vacuum.

Before the preparation of Fe_3O_4@MIP, OFX (78.6 mg, 0.2 mmol) and AA (137.4 μL, 2.0 mmol) were dissolved in acetonitrile (20 mL) and the solution was stirred for 12 h. Then, Fe_3O_4@TTCA nanoparticles (65.6 mg) were dispersed in the solution by ultrasonic vibration, followed by the addition of EGDMA (376 μL, 2.0 mmol) and AIBN (6.56 mg, 0.04 mmol). The mixture was purged with N_2 gas for 15 min while being cooled in an ice bath. The polymerization was carried out at 50 °C for 6 h and further at 65 °C for 18 h. The final product Fe_3O_4@MIP nanoparticles were separated and washed with

acetonitrile and methanol three times, respectively. The OFX template molecules existing in Fe_3O_4@MIP nanoparticles were removed with acetic acid-methanol (4:6, v/v) until no templates were detected in the supernatant by HPLC. After that, the Fe_3O_4@MIP nanoparticles were washed with ultrapure water until neutral and dried under vacuum.

The Fe_3O_4@NIP nanoparticles were prepared under the same conditions without the addition of the template OFX.

2.4. Characterization. X-ray photoelectron spectroscopy (XPS) data were obtained with an ESCALab220i-XL electron spectrometer from VG Scientific (London, UK) using 300 W AlK aradiation. Fourier transform infrared (FT-IR) spectroscopy characterization was performed with a Tensor-27 FT-IR spectrometer (Bruker, Germany). The spectra were scanned over a range of 4000−400 cm^{-1} in the transmission mode, accumulating 32 scans at a resolution of 4 cm^{-1}. Magnetic properties were determined with a 7410 vibrating sample magnetometer (VSM, Lake Shore, Cryotronics Inc., Ohio, USA). Morphological observation of the nanoparticles was carried out by JEM-2010 high resolution transmission electron microscope (JEOL, Tokyo, Japan). Thermogravimetric analysis was performed using Perkin−Elmer Pyris 1 TG analyzer (PE, USA) to determine the weight loss. X-ray diffraction (XRD) patterns were measured in the range of 2θ = 20−80° by step scanning on the Rigaku D/MAX-2500 diffractometer (Rigaku Co., Japan) with Cu Kα radiation.

2.5. HPLC Analysis. Chromatographic analysis was performed on a Shimadzu UFLC system (Shimadzu, Kyoto, Japan) consisting of two LC-20AD pumps, an SPD-M20A diode-array detector, a CTO-20A oven, and an SIL-20A auto sampler. The detection wavelengths were 294 nm for OFX and GAT, 278 nm for PEF, ENRO and NOR. For the analysis of individual compound, the mobile phase was acetonitrile-0.02 mol/L tetrabutyl ammonium bromide aqueous solution (12/88, v/v, pH 2.90). During the separation of mixed solutions of FQs, the mobile phase was acetonitrile-0.02 mol/L tetrabutyl ammonium bromide aqueous solution containing 0.06% trifluoroacetic acid (12/88, v/v). The flow rate was 1.0 mL/min. For the analysis of BPA, the detection wavelength was 278 nm, and the mobile phase was acetonitrile−water (60/40, v/v). For SMO, the detection wavelength was 278 nm, and the mobile phase was methanol (0.1% acetic acid)-water (0.1% acetic acid) (30/70, v/v). During the separation of BPA, SMO from FQs in the mixed solutions, the mobile phase was acetonitrile−water (0.1% formic acid) (40/60, v/v). A Dikma Diamonsil C_{18} column (250 mm × 4.6 mm, 5 μm, Dikma Technologies Inc., Beijing, China) was used throughout.

2.6. Binding Experiments. To evaluate the recognition properties of Fe_3O_4@MIP and Fe_3O_4@NIP nanoparticles, we performed the adsorption experiments as follows.

Static equilibrium experiments were carried out by mixing Fe_3O_4@MIP nanoparticles (4.0 mg) with OFX acetonitrile solutions (2.0 mL) in screw-capped glass tubes. The OFX concentrations were varied from 0.01 to 0.8 mmol/L. All the tubes were sealed and shaked in an incubator at 25 °C for 1 h. After incubation, the Fe_3O_4@MIP nanoparticles were separated by an external magnetic field. The concentrations of OFX in supernatants were determined by RP-HPLC. The same procedure was performed for Fe_3O_4@NIP.

The equilibrium binding amounts of OFX were calculated according to the equation: $Q = (C_i - C_f)V/m$, where Q (μmol/g) is the equilibrium binding amount of OFX, C_i (μmol/L) is the initial concentration of OFX, C_f (μmol/L) is the final concentration of OFX, V (mL) is the total volume of the adsorption mixture, and m (mg) is the mass of Fe_3O_4@MIP or Fe_3O_4@NIP.

In the adsorption kinetics experiments, Fe_3O_4@MIP (4.0 mg) was added into OFX solution (2.0 mL) with a concentration of 0.8 mmol/L and incubated at 25 °C for different time intervals: 10, 20, 30, 40, 60, 90, and 120 min, respectively. After incubation, the Fe_3O_4@MIP was separated by an external magnetic field and the OFX concentrations of supernatant solutions were determined by RP-HPLC.

In the selectivity experiments, NOR, GAT, PEF, and ENRO were chosen as structural analogues. Fe_3O_4@MIP (4.0 mg) was dispersed in the solutions of OFX and five structural analogues (0.5 mmol/L, 2.0 mL), respectively. The mixtures were incubated at 25 °C for 1 h. The concentration of each compound in supernatant solution was then determined by RP-HPLC. In addition, BPA and SMO were also used as nonstructural analogues to evaluate the selectivity of Fe_3O_4@MIP nanoparticles. The same procedure was applied to Fe_3O_4@NIP.

For the competitive binding assay, five FQs (OFX, NOR, GAT, PEF, and ENRO) were mixed with nonstructural analogues SMO and BPA in acetonitrile. The concentration of each compound was 50 μmol/L. Fe_3O_4@MIP (10 mg) was dispersed in the above mixture of 1.0 mL. After incubated for 1 h at room temperature, the supernatant was analyzed by RP-HPLC to evaluate the competitive binding amounts of each compound. All tests were conducted in triplicate.

2.7. Determination of Five FQs in Human Urine. The human urine samples were acquired from a healthy volunteer. Without any pretreatment, human urine (2.0 mL) was spiked with five FQs (OFX, NOR, GAT, PEF, and ENRO) at three concentration levels of 0.05, 0.1, and 1.0 μg/mL, respectively. The FQs spiked urine samples were homogenized in a shaker at 25 °C for 15 min. And then Fe_3O_4@MIP nanoparticles (50 mg) were added into the three urine samples, respectively. After the mixtures were incubated at 25 °C for 2 h, the Fe_3O_4@MIP nanoparticles were separated by a magnet and washed with ultrapure water (2 mL) twice. Then extracted fractions were eluted by acetic acid-methanol (4 mL, 4:6, v/v). The eluants were dried with N_2 gas. The residues were redissolved with mobile phase (0.5 mL) and analyzed by RP-HPLC.

3. RESULTS AND DISCUSSION

3.1. Preparation of OFX-Imprinted Fe_3O_4@MIP Nanoparticles. The procedure of preparing OFX-imprinted Fe_3O_4@MIP is depicted in Scheme 1. Fe_3O_4 nanoparticles

Scheme 1. Procedure of Preparing OFX-Imprinted Fe_3O_4@MIPs

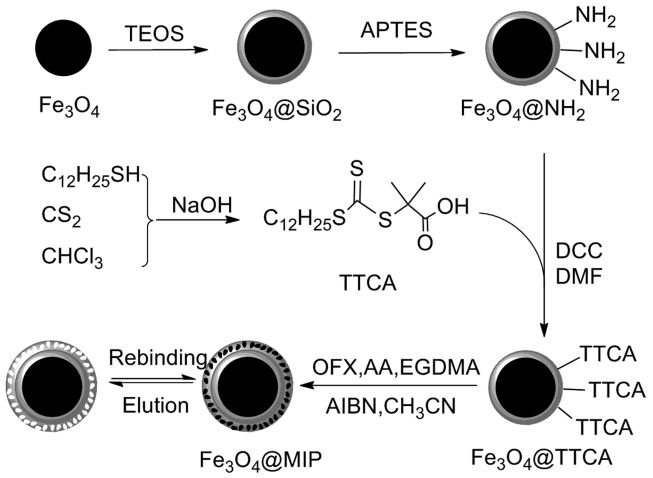

were synthesized as the magnetic core, which made the MIP material magnetic-responsive and easily controlled during separation. The coating of Fe_3O_4 core with SiO_2 shell enabled easy functionalization of amino group and further grafting of the RAFT agent TTCA. The ESI MS and ^{1}H NMR characterization data of TTCA were shown in Figures S1 and S2 in the Supporting Information. In the polymerization, the initiator of AIBN was added into the reaction solution to induce the surface polymerization.[35] With the RAFT agent TTCA modified on the surface of SiO_2 shell, the MIP layer could be grafted from the inorganic SiO_2 surface. According to the literature,[23,36] a two-step-temperature polymerization was employed for the preparation of the nanoscale MIP layer. At lower temperature of 50 °C, polymerization occurred at a slower rate. Because of the high chain-transfer efficiency of the RAFT agent TTCA,[31] the initial oligomer layer was formed on

the surface of TTCA modified SiO_2 shell. When elevating the reaction temperature to 65 °C, the oligomers was induced to grow and finally form the OFX-imprinted polymer shell.

To obtain more effective MIP layer, the kinds of functional monomers and the ratio of functional monomer to cross-linker were further optimized. Benefiting from the good compatibility of RAFT toward a wide range of monomers, acidic monomers MAA and AA that can act as hydrogen-bond donor were chosen to prepare the OFX imprinted MIPs. The binding properties of the MIPs were estimated and compared via the imprinted factor (IF).

$$IF = Q_{MIP}/Q_{NIP}$$

where Q_{MIP} is the amount of OFX bound to the MIPs, Q_{NIP} is the amount of OFX bound to the NIPs. With the same monomer-to-cross-linker ratio (1:1), the IF values, calculated from the ratio of binding amounts of OFX on MIP and NIP, are 6.0 and 1.8 for AA and MAA related polymers, respectively. The MIPs prepared from AA shows significantly better binding efficiency toward OFX than those obtained from MAA (Figure 1). Moreover, the molar ratio of AA to EGDMA was

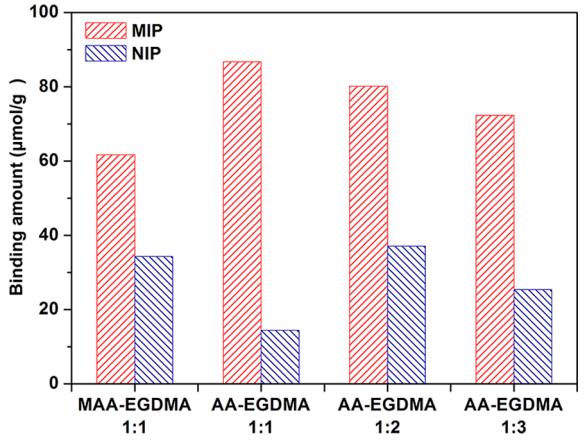

Figure 1. Binding amounts of OFX on Fe_3O_4@MIP and Fe_3O_4@NIP at different preparing conditions.

investigated at 1:1, 1:2 and 1:3. Correspondingly, the binding amounts of OFX on MIPs are 86.8, 80.1, and 72.3 μmol/g and the values of IF are 6.0, 2.2, and 2.9, respectively. According to the results of binding experiments, the MIPs prepared at 1:1 shows both highest binding ability and imprinted factor. Hence, AA was chosen as the functional monomer and the ratio of AA to EGDMA was set as 1:1.

On the basis of the results from optimization of preparation conditions, recognition mechanism can be discussed. During the preparation of MIP, the copolymerization of the monomer acrylic acid and cross-linker EGDMA in the presence of template ofloxacin created the specific recognition cavities. The cross-linking enables the maintenance of three-dimensional structure complementary to the template molecules in size and shape. The results that Fe_3O_4@MIP possesses significant higher binding ability for ofloxacin than Fe_3O_4@NIP clarify the contribution from shape recognition in the imprinting process. More importantly, chemical functionality also contributed for the recognition. Hydrogen bonding can be formed at the sites of F atoms, O atoms of carbonyl group, and carboxyl group of OFX.[31] Because ofloxacin consisting of 6-fluoro, 7-piperazinyl, and 3-carboxyl are hydrophilic zwitterions, ion interactions may be also included in the recognition between the MIP and the template.[37] By adjusting the pH of the environmental solution, the binding of ofloxacin on MIP materials can be easily controlled.

3.2. Characterization of Fe_3O_4, Fe_3O_4@SiO_2 and Fe_3O_4@MIP Nanoparticles. *3.2.1. Morphological Characterization.* TEM was utilized to observe the morphological features of Fe_3O_4, Fe_3O_4@SiO_2, and Fe_3O_4@MIP nanoparticles. Fe_3O_4 nanoparticles exhibited the spherical shape with the mean diameter of 400 nm (Figure 2a, b). After SiO_2

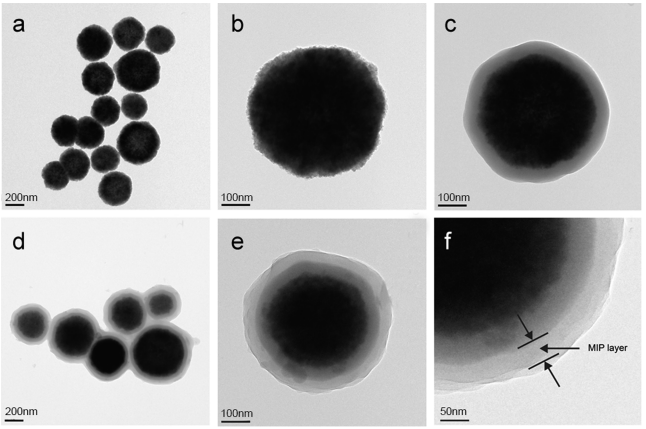

Figure 2. TEM images of (a, b) Fe_3O_4, (c) Fe_3O_4@SiO_2, (d, e) Fe_3O_4@MIP, and (f) MIP layer of Fe_3O_4@MIP.

modification and MIP grafting, both the Fe_3O_4@SiO_2 and Fe_3O_4@MIP still remained the fine spherical morphology (Figure 2c–e and Figure S3 in the Supporting Information). It is worth mentioning that the well-defined core–shell structures can be obviously observed for Fe_3O_4@SiO_2 and Fe_3O_4@MIP nanoparticles. The core with dark contrast represented the Fe_3O_4 nanoparticle; the inner layer with medium contrast represented the SiO_2 shell; the outer layer with light contrast represented the MIP shell. From the TEM image of Fe_3O_4@SiO_2 (Figure 2c), the thickness of the silica layer is about 50 nm, clearly showing that the Fe_3O_4 nanoparticles were fully coated by silica. By varying the TEOS concentration in the reaction, the thickness of the silica layer can be well controlled. Benefiting from the characteristic superiority of RAFT reaction in controllable and living polymerization, uniform MIP shell with an average thickness of 50 nm was very evenly grafted on the SiO_2 shell (Figure 2e, f). Such fine core–shell structure was favorable for the fast mass transfer during template binding and removing.

3.2.2. Magnetic Properties. Magnetic property is crucial to magnetic nanoparticles for their applications in fast separation. The magnetic properties of Fe_3O_4, Fe_3O_4@SiO_2, and Fe_3O_4@MIP nanoparticles were measured by VSM. As shown in Figure 3, the saturation magnetization of Fe_3O_4, Fe_3O_4@SiO_2, and Fe_3O_4@MIP were 68.8, 43.9, and 22.6 emu/g, respectively. Even if the magnetic response of Fe_3O_4@MIP nanoparticles decreased to 22.6 emu/g after the formation of SiO_2 and MIP layers, such magnetic nanoparticles still possess high magnetization and can be rapidly and completely separated from the mixture by an external magnetic field within 10 s. Also from Figure 3, there was no magnetic hysteresis for all three kinds of nanoparticles, indicating Fe_3O_4, Fe_3O_4@SiO_2, and Fe_3O_4@MIP nanoparticles show superparamagnetic behavior. The super-

dx.doi.org/10.1021/am5020666 | ACS Appl. Mater. Interfaces 2014, 6, 9634–9642

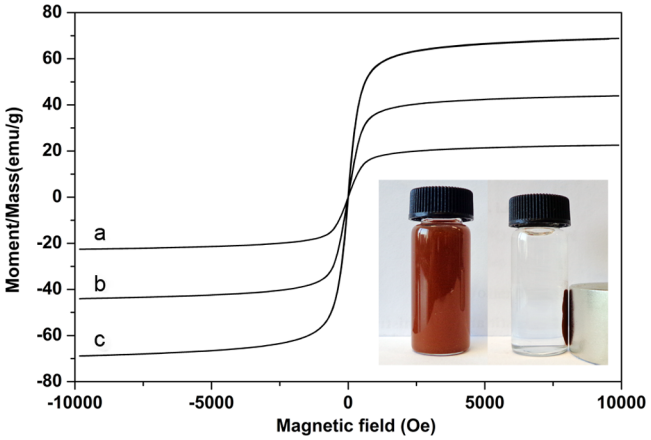

Figure 3. VSM curves of (a) Fe_3O_4@MIP, (b) Fe_3O_4@SiO_2, and (c) Fe_3O_4 nanoparticles. The inset shows a solution of Fe_3O_4@MIP in the absence (left) and the presence (right) of a magnet.

paramagnetism could make the Fe_3O_4@MIP nanoparticles quick aggregation as well as stable and homogeneous suspension with and without an external magnet during practical application.

3.2.3. FT-IR Characterization. The FT-IR spectra of Fe_3O_4, Fe_3O_4@SiO_2, and Fe_3O_4@MIP are shown in Figure 4.

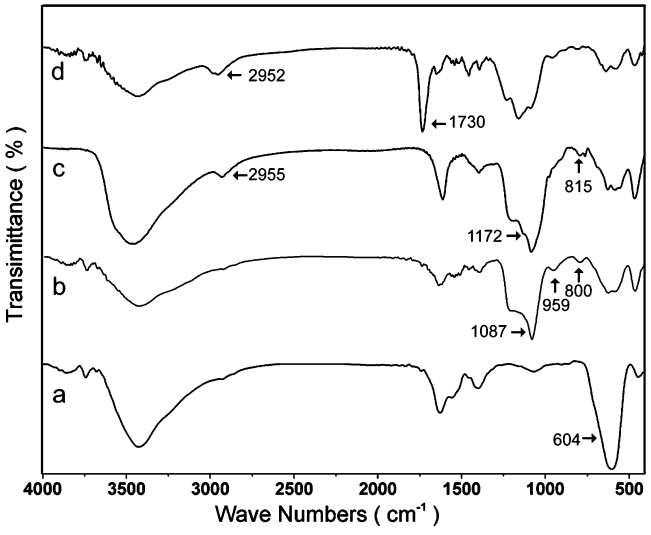

Figure 4. FT-IR spectra of (a) Fe_3O_4, (b) Fe_3O_4@SiO_2, (c) TTCA-grafted Fe_3O_4, and (d) Fe_3O_4@MIP nanoparticles.

Obviously, the characteristic absorption band of Fe_3O_4 appeared at 604 cm^{-1}. The peaks at 959, 800, and 1087 cm^{-1} are attributed to the stretching vibration of Si−O−H, Si−O, and Si−O−Si, respectively. The IR absorption of Fe_3O_4@SiO_2 indicated that the SiO_2 layer was encapsulated on the surface of Fe_3O_4 nanoparticles. After TTCA grafting, the appearance of three new peaks at 815, 1172, and 2955 cm^{-1} were attributed to the stretching vibration of C−S and C═S. the stretching vibration of C−H, respectively. Two new peaks at 1730 and 2952 cm^{-1} from Fe_3O_4@MIP were attributed to the stretching vibration of C═O and C−H, which confirmed that the MIP layer was successfully grafted on the surface of Fe_3O_4@SiO_2.

3.2.4. XPS Characterization. To further illustrate the successful anchor of -NH_2 and TTCA on the surface of nanoparticles, XPS was used to characterize the chemical composition of the surface of Fe_3O_4@NH_2 and Fe_3O_4@TTCA. As shown in Figure S4 in the Supporting Information, characteristic peaks for silicon (Si 2p), carbon (C 1s), nitrogen (N 1s) and oxygen (O 1s) were clearly detected at 103.2, 284.8, 399.2, and 532.4 eV. The appearance of nitrogen (N 1s) (Figure S4A inset) proved that the -NH_2 was modified on the surface of Fe_3O_4@SiO_2 nanoparticles. In the next step of coupling with TTCA, the successful reaction between −NH_2 and TTCA was affirmed by the appearance of an S_{2p} signal of 163.5 eV (see Figure S4B inset in the Supporting Information).

3.2.5. Thermogravimetric Analysis. The thermogravimetric analysis was performed to further estimate the grafting yield of imprinted polymer layer on Fe_3O_4@MIP nanoparticles. Figure 5 reveals the TGA curves of Fe_3O_4, Fe_3O_4@SiO_2 and Fe_3O_4@

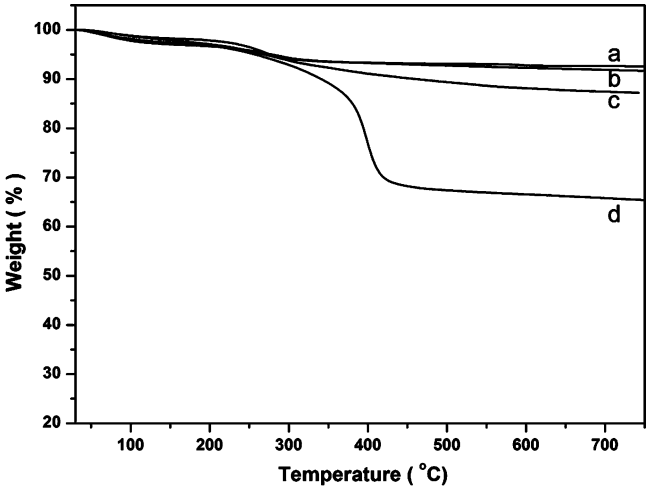

Figure 5. TGA curves of (a) Fe_3O_4, (b) Fe_3O_4@SiO_2, (c) TTCA-grafted Fe_3O_4, and (d) Fe_3O_4@MIP nanoparticles.

MIP in the temperature range of 25−750 °C. Clearly, during the successive heating process, the mass changes are very slight for Fe_3O_4 and Fe_3O_4@SiO_2. At 750 °C, the mass losses of Fe_3O_4 and Fe_3O_4@SiO_2 are 7.2 and 8 wt %, respectively, indicating the stability of these nanoparticles. For the TTCA-grafted nanoparticles, a mass loss of 12.8% was found after continuous heating (Figure 5c), indicating the successful modification of the RAFT agent. In contrast, dramatic mass change was detected for Fe_3O_4@MIP. The MIP polymer layer began to thermally decompose at about 270 °C, accompanied by a significant mass loss.[38] The mass loss continued up to about 450 °C, after that, the mass kept relatively constant. The total mass loss of Fe_3O_4@MIP reaches to 34.2 wt % until 750 °C. The results revealed the grafting of imprinted polymer on the surface of Fe_3O_4@SiO_2 was successful and effective.

3.2.6. XRD Determination. XRD was performed to obtain the crystalline structure of Fe_3O_4, Fe_3O_4@SiO_2 and Fe_3O_4@MIP nanoparticles. The X-ray diffraction pattern for the standard Fe_3O_4 crystal has six diffraction peaks: (220), (311), (400), (422), (511), and (440). As shown in Figure S5 (Supporting Information), the XRD patterns of Fe_3O_4 nanoparticles prepared via solvothermal method agreed well with that of the standard magnetite.[32] After coated with SiO_2 and MIP layer, Fe_3O_4@SiO_2 and Fe_3O_4@MIP nanoparticles still showed the same XRD signals at (220), (311), (400), (422), (511), and (440), suggesting that the process of preparation SiO_2 and MIP layer did not affect the crystal structure of the magnetite core.

dx.doi.org/10.1021/am5020666 | ACS Appl. Mater. Interfaces 2014, 6, 9634−9642

3.3. Absorption Kinetics of Fe_3O_4@MIP Nanoparticles. The absorption kinetics of Fe_3O_4@MIP nanoparticles is one of the key factors for fast separation in practical application. The results are shown in Figure 6. Only after 10 min adsorption, the

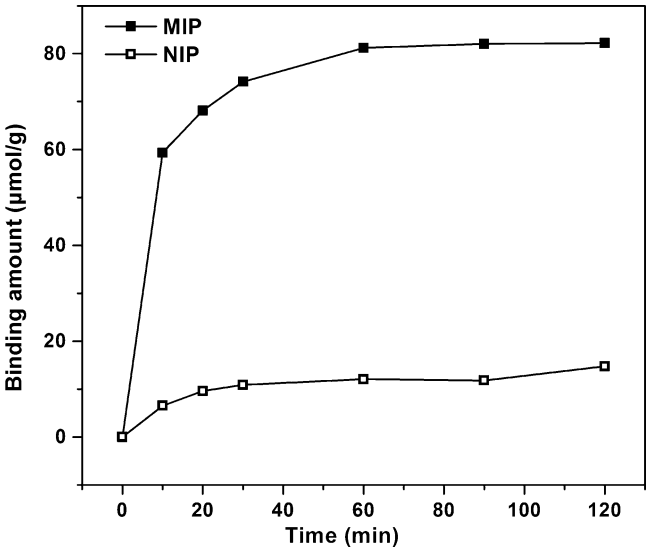

Figure 6. Adsorption kinetics curves of OFX on Fe_3O_4@MIP and Fe_3O_4@NIP.

binding amount of OFX on Fe_3O_4@MIP greatly increased to 58 μmol/g, which is 75% of the total equilibrium binding amount. As the binding period prolonged, the binding amount slowly increased. After adsorption for 60 min, the binding amount of OFX increased to 78 μmol/g and reached the adsorption equilibrium. In comparison, the MIPs prepared by the conventional method of bulk polymerization took more than 10 h to reach the absorption equilibrium.[39] The surface imprinted MIP nanoparticles exhibited significantly shorter equilibrium time. The 50 nm-thick imprinted layer at the surface of Fe_3O_4@MIP nanoparticles makes the imprinted sites more accessible, which is beneficial for easier binding and removal of template molecule OFX. The adsorption kinetic of Fe_3O_4@NIP nanoparticles was also examined. The binding amount of OFX on Fe_3O_4@NIP kept very low as the adsorption time prolonged, further demonstrating the high selectivity of imprinted layer. The absorption time of 60 min was chosen for charactering Fe_3O_4@MIP and Fe_3O_4@NIP nanoparticles.

3.4. Absorption Capacity of Fe_3O_4@MIP and Fe_3O_4@NIP Nanoparticles. The static equilibrium experiments were carried out to evaluate the absorption capacity of Fe_3O_4@MIP and Fe_3O_4@NIP. As show in Figure 7, the binding amounts of OFX on Fe_3O_4@MIP and Fe_3O_4@NIP increased with the increasing initial concentration of OFX solution. When the concentration of OFX was 0.6 mmol/L, the binding amount of OFX achieved a nearly saturated plateau and no obvious increase was observed with higher concentration of 0.8 mmol/L. The Fe_3O_4@MIP revealed highly specific binding ability to the template OFX than Fe_3O_4@NIP.

In order to quantitatively estimate the binding properties of Fe_3O_4@MIP and Fe_3O_4@NIP nanoparticles, the data obtained from static absorption experiments were further processed with Scatchard analysis based on the equation:[40] $Q/C_e = Q_{max}/K_d - Q/K_d$, where Q and Q_{max} were the experimental adsorption capacity (μmol/g) of OFX and the theoretical maximum

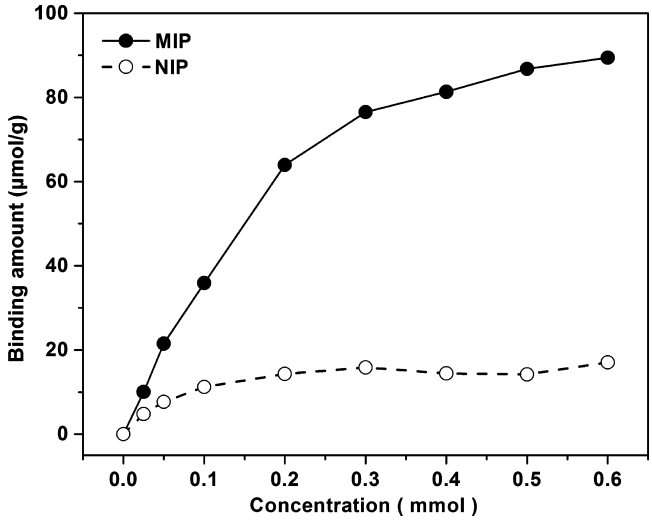

Figure 7. Adsorption isotherm curves of OFX on Fe_3O_4@MIP and Fe_3O_4@NIP nanoparticles.

adsorption capacity of the polymer (μmol/g), respectively, C_e was the concentration of OFX in equilibrium solution (μmol/L), and K_d is the dissociation constant (μmol/L). The values of K_d and Q_{max} can be calculated from the slope and intercept of the linear equation plotted in Q/C_e versus Q. The saturated adsorption capacity of the Fe_3O_4@MIP for OFX was 90.5 μmol/g with a dissociation constant of 23.2 μmol/L and the saturated adsorption capacity of the Fe_3O_4@NIP for OFX was 18.2 μmol/g with a dissociation constant of 45.6 μmol/L. The results indicated that the Fe_3O_4@MIP nanoparticles had much stronger ability to distinguish the template molecule OFX than the Fe_3O_4@NIP ones.

3.5. Selectivity of Fe_3O_4@MIP Nanoparticles. To investigate the selectivity of Fe_3O_4@MIP nanoparticles for FQs, we dispersed MIP and NIP nanoparticles in each solution of five FQs including OFX, ENRO, PEF, NOR, and GAT, respectively. As the control, SMO and BPA were chosen as the reference compounds and subjected to the same treatment. The chemical structures of these analytes are shown in Figure S6 in the Supporting Information. The initial concentrations of FQs were all 0.5 mmol/L. As displayed in Figure 8, all five FQs were well recognized by Fe_3O_4@MIP with high binding amount whereas obvious lower adsorption was detected on Fe_3O_4@NIP. For SMO and BPA, negligible binding was observed on both Fe_3O_4@MIP and Fe_3O_4@NIP nanoparticles. IF values were also calculated based on these data. The IF values for OFX, ENRO, PEF, NOR and GAT were determined as 6.0, 2.0, 1.2, 2.6, and 2.5, respectively. The imprinted effect, molecular interactions and specific structures may contribute to the selectivity of Fe_3O_4@MIP.

Competitive binding assay was also performed to further verify the recognition ability of Fe_3O_4@MIP toward FQs. OFX, ENRO, PEF, NOR and GAT were mixed with SMO and BPA with equalmolar amounts. The mixture solution was incubated with Fe_3O_4@MIP nanoparticles for adsorption. As shown in Figure 9, five FQs showed high binding affinity on Fe_3O_4@MIP nanoparticles. In contrast, almost no adsorption of SMO and BPA was detected. These results demonstrate that Fe_3O_4@MIP is able to discriminate five FQs from interference compounds SMO and BPA. Benefiting from such high selectivity, Fe_3O_4@MIP nanoparticles were expected to simultaneously recognition and enrichment of FQs in complex real samples.

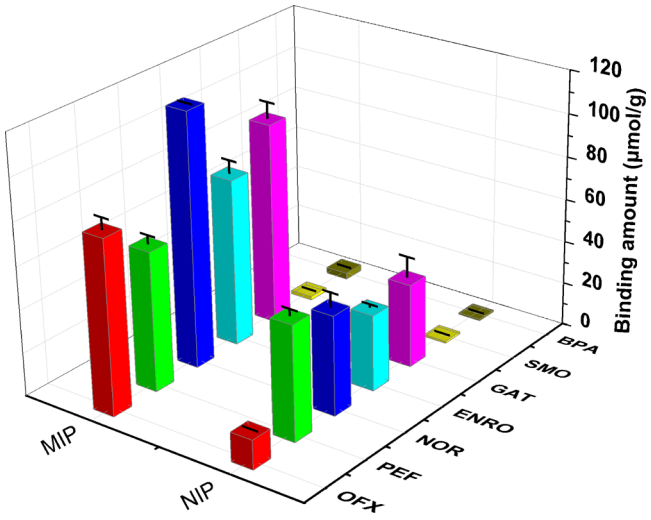

Figure 8. Binding behaviors of FQs and SMO, BPA on Fe_3O_4@MIP and Fe_3O_4@NIP.

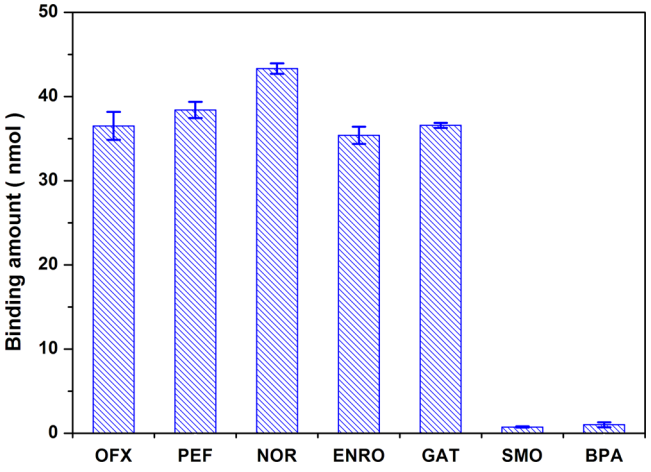

Figure 9. Competitive binding assay of FQs and SMO, BPA on Fe_3O_4@MIP.

According to the structures of these compounds, the characteristic skeleton structure of FQs plays important roles in the specific recognition mechanism. During the preparation of MIP, recognition cavities with three-dimensional structure and chemical functionalities were created. Besides size and shape recognition, hydrogen bonding and ionic interaction also play important roles. With same skeleton structure and thus similar steric shape and size, OFX, ENRO, PEF, NOR, and GAT showed very close binding ability to the imprinted cavities. Moreover, fluorine and oxygen atoms which these FQs have in common can form hydrogen bonds with hydrogen atom of carboxyl group in acrylic acid. Without these recognition elements, SMO and BPA with totally different structures cannot bind the MIP.

3.6. Determination of FQs in Human Urine. The prepared Fe_3O_4@MIP nanoparticles were used as the materials of solid phase extraction to selectively extract FQs of OFX, ENRO, PEF, NOR, and GAT in human urine samples, followed by RP-HPLC determination. Considering the low concentration of FQs and the complicated matrix in real samples, the absorption time of 120 min was selected so as to achieve sufficient adsorption equilibrium in real sample analyses. With the optimized HPLC method, the five FQs were baseline separated as shown in the chromatogram of Figure 10a. The linearities for the determination of five FQs

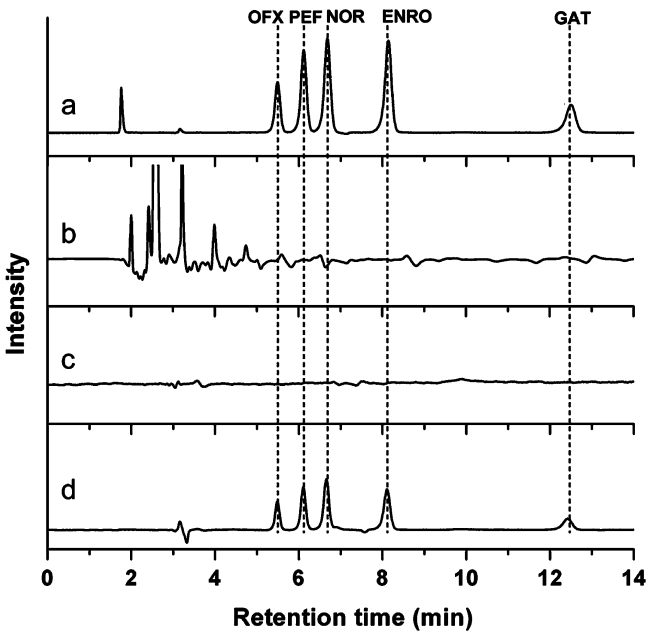

Figure 10. Chromatograms of (a) standard mixed solution of five FQs (OFX, PEF, NOR, ENRO and GAT), (b) FQs (OFX, PEF, NOR, ENRO, and GAT) spiked human urine without pre-enrichment by Fe_3O_4@MIP, (c) blank human urine after Fe_3O_4@MIP extraction, (d) FQs (OFX, PEF, NOR, ENRO, and GAT) spiked human urine after Fe_3O_4@MIP extraction. HPLC conditions: the mobile phase was acetonitrile-0.02 mol/L tetrabutyl ammonium bromide aqueous solution containing 0.06% TFA (12/88, v/v); the flow rate was 1.0 mL/min.

were estimated over the range of 0.1−100 μg/mL with a correlation coefficient of 0.999. According to the signal-to-noise of 3, the limits of detection for OFX, PEF, NOR, ENRO and GAT were 10.5, 12.0, 9.1, 19.4, and 8.5 ng/mL, respectively.

Human urine was spiked with five FQs at three different concentrations of 0.05, 0.10, and 1.00 μg/mL. Without any pretreatments, the Fe_3O_4@MIP nanoparticles were directly placed into the healthy human urine samples. After the adsorption for 2 h, the Fe_3O_4@MIP nanoparticles were collected by the magnet and then washed twice with water to remove the impurities. Then the enriched FQs were eluted from Fe_3O_4@MIP and analyzed by RP-HPLC. The chromatograms were illustrated in Figure 10. It can be seen that no peaks of FQs occurred when the FQs spiked urine sample was directly detected without MIP pre-enrichment, owing to the low spiked concentration of FQs (Figure 10b). The blank urine sample was also treated with Fe_3O_4@MIP (Figure 10c). Obviously, the impurities of urine sample presented in Figure 10b were eliminated and no peaks of FQs were detected. After the FQs spiked urine sample was treated with Fe_3O_4@MIP, the FQs were concentrated, resulting in the obvious peaks of FQs exhibited in Figure 10d. The amounts of the spiked and determined FQs in human urine were exhibited in Table 1. Clearly, when the concentrations of FQs were between 0.05 to 1.00 μg/mL, the recoveries were 83.1−103.1% with RSD of 0.8−8.2% (n = 3). These results demonstrated that the Fe_3O_4@

dx.doi.org/10.1021/am5020666 | ACS Appl. Mater. Interfaces 2014, 6, 9634−9642

Table 1. Recoveries of Five FQs Obtained from Human Urine Samples

		0.05 μg/mL		0.1 μg/mL		1.0 μg/mL	
sample	compd	recovery (%)	RSD (%)	recovery (%)	RSD (%)	recovery (%)	RSD (%)
human urine	OFX	94.2	5.6	100.2	2.4	95.3	3.0
	PEF	83.1	8.2	83.5	1.6	86.3	4.2
	NOR	83.3	7.7	85.6	0.8	84.6	3.6
	ENRO	85.5	3.0	99.3	1.1	85.5	3.2
	GAT	98.6	5.6	103.1	4.3	92.6	4.4

MIP nanoparticles can be utilized to directly and effectively separate and enrich FQs in real samples.

4. CONCLUSION

On the basis of the surface imprinting strategy, the novel magnetic imprinted core−shell Fe_3O_4@MIP nanoparticles were prepared via RAFT polymerization for the analysis of FQs. Because of the controlled property of RAFT, the uniform surface imprinted shell was successfully constructed on the surface of Fe_3O_4@SiO_2. The surface imprinted MIPs reveal high binding capacity, short absorption equilibrium time and specific recognition toward FQs. The Fe_3O_4@MIP nanoparticles also exhibited a desired level of magnetic susceptibility, resulting in the convenient and highly efficient extraction. The Fe_3O_4@MIP nanoparticles were directly and successfully utilized to extract five FQs from human urine samples with satisfactory recoveries and reproducibility. The well-constructed core−shell MIP nanoparticles reveal the great prospect for enrichment and separation of such drugs in complicated matrixes.

■ ASSOCIATED CONTENT

Supporting Information

Mass spectroscopy and ^{1}H NMR spectra of TTCA. XPS and XRD characterization. Molecular structures of fluoroquinolones and SMO, BPA. IF values of six fluoroquinolones. This material is available free of charge via the Internet at http://pubs.acs.org.

■ AUTHOR INFORMATION

Corresponding Authors

*E-mail: zhaorui@iccas.ac.cn. Tel: +86 10 62557910. Fax: +86 10 62559373.

*E-mail: yyhuang@iccas.ac.cn..

Notes

The authors declare no competing financial interest.

■ ACKNOWLEDGMENTS

The authors are appreciated the financial supports from National Natural Science Foundation of China (21375134, 21105105, 21135006 and 21321003) and Institute of Chemistry, Chinese Academy of Sciences (CMS-PY-201214).

■ REFERENCES

(1) Chen, L.; Xu, S.; Li, J. Recent Advances in Molecular Imprinting Technology: Current Status, Challenges and Highlighted Applications. *Chem. Soc. Rev.* **2011**, *40*, 2922−2942.

(2) Michael, J. W.; Iva, C.; Lee, L.; Sergey, A.; Piletsky, J. N.; Robert, P.; Adrian, H. The Rational Development of Molecularly Imprinted Polymer−Based Sensors for Protein Detection. *Chem. Soc. Rev.* **2011**, *40*, 1547−1571.

(3) Vlatakis, G.; Andersson, L. I.; Muller, R.; Mosbach, K. Drug Assay Using Antibody Mimics Made by Molecular Imprinting. *Nature* **1993**, *361*, 645−647.

(4) Wulff, G. Enzyme−like Catalysis by Molecularly Imprinted Polymers. *Chem. Rev.* **2002**, *102*, 1−28.

(5) Zhou, W.; Tang, S.; Yao, Q.; Chen, F.; Yang, H.; Wang, X. A Quartz Crystal Microbalance Sensor Based on Mussel−Inspired Molecularly Imprinted Polymer. *Biosens. Bioelectron.* **2010**, *26*, 585−589.

(6) Li, J.; Li, Y.; Zhang, Y.; Ge, W. Highly Sensitive Molecularly Imprinted Electrochemical Sensor Based on the Double Amplification by an Inorganic Prussian Blue Catalytic Polymer and the Enzymatic Effect of Glucose Oxidase. *Anal. Chem.* **2012**, *84*, 1888−1893.

(7) Zhong, Q.; Hu, Y.; Li, G. Dynamic Liquid-liquid-solid Microextraction Based on Molecularly Imprinted Polymer Filaments on−line Coupling to High Performance Liquid Chromatography for Direct Analysis of Estrogens in Complex Samples. *J. Chromatogr. A* **2012**, *1241*, 13−20.

(8) Hu, Y.; Song, C.; Li, G. Fiber−in−Tube Solid−Phase Microextraction with Molecularly Imprinted Coating for Sensitive Analysis of Antibiotic Drugs by High Performance Liquid Chromatography. *J. Chromatogr. A* **2012**, *1263*, 21−27.

(9) Lenain, P.; Mavungu, J. D. D.; Dubruel, P.; Robbens, J.; Saeger, S. D. Development of Suspension Polymerized Molecularly Imprinted Beads with Metergoline as Template and Application in a Solid−Phase Extraction Procedure toward Ergot Alkaloids. *Anal. Chem.* **2012**, *84*, 10411−10418.

(10) Cai, X.; Li, J.; Zhang, Z.; Yang, F..; Dong, R.; Chen, L. Novel Pb^{2+} Ion Imprinted Polymers Based on Ionic Interaction via Synergy of Dual Functional Monomers for Selective Solid−Phase Extraction of Pb^{2+} in Water Samples. *ACS Appl. Mater. Interfaces* **2014**, *6*, 305−313.

(11) Wulff, G.; Liu, J. Design of Biomimetic Catalysts by Molecular Imprinting in Synthetic Polymers: the Role of Transition State Stabilization. *Acc. Chem. Res.* **2012**, *45*, 239−247.

(12) Shen, X.; Zhu, L.; Li, J.; Tang, H. Synthesis of Molecular Imprinted Polymer Coated Photocatalysts with High Selectivity. *Chem. Commun.* **2007**, 1163−1165.

(13) Zheng, C.; Zhang, X.; Liu, W.; Liu, B.; Yang, H.; Lin, Z.; Chen, G. A Selective Artificial Enzyme Inhibitor Based on Nanoparticle−Enzyme Interactions and Molecular Imprinting. *Adv. Mater.* **2013**, *25*, 5922−5927.

(14) Hoshino, Y.; Yoshio, T.; Okahata, K.; Shea, K. J. Peptide Imprinted Polymer Nanoparticles: a Plastic Antibody. *J. Am. Chem. Soc.* **2008**, *130*, 15242−15243.

(15) Chianella, I.; Guerreiro, A.; Moczko, E.; Caygill, J. S.; Piletska, E. V.; Sansalvador, I. M. P. D. V.; Whitcombe, M. J.; Piletsky, S. A. Direct Replacement of Antibodies with Molecularly Imprinted Polymer Nanoparticles in ELISA Development of a Novel Assay for Vancomycin. *Anal. Chem.* **2013**, *85*, 8462−8468.

(16) Liu, Y.; He, Y.; Jin, Y.; Huang, Y.; Liu, G.; Zhao, R. Preparation of Monodispersed Macroporous Core-Shell Molecularly Imprinted Particles and Their Application in the Determination of 2,4-Dichlorophenoxyacetic Acid. *J. Chromatogr. A* **2014**, *1323*, 11−17.

(17) Li, D.; He, X.; Chen, Y.; Li, W.; Zhang, Y. Novel Hybrid Structure Silica/CdTe/Molecularly Imprinted Polymer: Synthesis, Specific Recognition, and Quantitative Fluorescence Detection of Bovine Hemoglobin. *ACS Appl. Mater. Interfaces* **2013**, *5*, 12609−12616.

(18) Xu, C.; Uddin, K. M. A.; Shen, X.; Jayawardena, S. N. H.; Yan, M.; Ye, L. Photoconjugation of Molecularly Imprinted Polymer with

Magnetic Nanoparticles. *ACS Appl. Mater. Interfaces* **2013**, *5*, 5208−5213.
(19) Lee, M.; Thomas, J. L.; Chen, Y.; Wang, H.; Lin, H. Hydrolysis of Magnetic Amylase-Imprinted Poly(Ethylene-co-Vinyl Alcohol) Composite Nanoparticles. *ACS Appl. Mater. Interfaces* **2012**, *4*, 916−921.
(20) Lee, M.; Thomas, J. L.; Ho, M.; Yuan, C.; Lin, H. Synthesis of Magnetic Molecularly Imprinted Poly(Ethylene-co-Vinyl Alcohol) Nanoparticles and Their Uses in the Extraction and Sensing of Target Molecules in Urine. *ACS Appl. Mater. Interfaces* **2010**, *2*, 1729−1736.
(21) Lu, C.; Wang, Y.; Li, Y.; Yang, H.; Chen, X.; Wang, X. Bifunctional Superparamagnetic Surface Molecularly Imprinted Polymer Core−Shell Nanoparticles. *J. Mater. Chem.* **2009**, *19*, 1077−1079.
(22) Liu, J.; Wang, W.; Xie, Y.; Huang, Y.; Liu, Y.; Liu, X.; Zhao, R.; Liu, G.; Chen, Y. A Novel Polychloromethylstyrene Coated Superparamagnetic Surface Molecularly Imprinted Core−Shell Nanoparticle for Bisphenol A. *J. Mater. Chem.* **2011**, *21*, 9232−9238.
(23) Xu, S.; Li, J.; Chen, L. Molecularly Imprinted Core−Shell Nanoparticles for Determination of Trace Atrazine by Reversible Addition−Fragmentation Chain Transfer Surface Imprinting. *J. Mater. Chem.* **2011**, *21*, 4346−4351.
(24) Moraes, J.; Ohno, K.; Maschmeyer, T.; Perrier, S. Synthesis of Silica−polymer Core−shell Nanoparticles by Reversible Addition−Fragmentation Chain Transfer Polymerization. *Chem. Commun.* **2013**, *49*, 9077−9088.
(25) Bompart, M.; Haupt, K. Molecularly Imprinted Polymers and Controlled/Living Radical Polymerization. *Aust. J. Chem.* **2009**, *62*, 751−761.
(26) Nelson, J. M.; Chiller, T. M.; Powers, J. H.; Angulo, F. J. Fluoroquinolone−Resistant Campylobacter Species and the Withdrawal of Fluoroquinolones from Use in Poultry: A Public Health Success Story. *Clin. Infect. Dis.* **2007**, *44*, 977−980.
(27) Kantiani, L.; Farre, M.; Barcelo, D. Rapid Residue Analysis of Fluoroquinolones in Raw Bovine Milk by Online Solid Phase Extraction Followed by Liquid Chromatography Coupled to Tandem Mass Spectrometry. *J. Chromatogr. A* **2011**, *1218*, 9019−9027.
(28) Zheng, M.; Gong, R.; Zhao, X.; Feng, Y. Selective Sample Pretreatment by Molecularly Imprinted Polymer Monolith for the Analysis of Fluoroquinolones from Milk Samples. *J. Chromatogr. A* **2010**, *1217*, 2075−2081.
(29) Xiao, D.; Dramou, P.; Xiong, N.; He, H.; Li, H.; Yuan, D.; Dai, H. Development of Novel Molecularly Imprinted Magnetic Solid−phase Extraction Materials Based on Magnetic Carbon Nanotubes and Their Application for the Determination of Gatifloxacin in Serum Samples Coupled with High Performance Liquid Chromatography. *J. Chromatogr. A* **2013**, *1274*, 44−53.
(30) Shi, Y.; Lv, H.; Lu, X.; Huang, Y.; Zhang, Y.; Xue, W. Uniform Molecularly Imprinted Poly(Methacrylic Acid) Nanospheres Prepared by Precipitation Polymerization: the Control of Particle Features Suitable for Sustained Release of Gatifloxacin. *J. Mater. Chem.* **2012**, *22*, 3889−3998.
(31) Sun, H.; Qiao, F. Recognition Mechanism of Water-Compatible Molecularly Imprinted Solid-Phase Extraction and Determination of Nine Quinolones in Urine by High Performance Liquid Chromatography. *J. Chromatogr. A* **2008**, *1212*, 1−9.
(32) John, T.; Lai, D.; Shea, R. Functional Polymers from Movel Carboxyl−terminated Trithiocarbonates as Highly Efficient RAFT Agents. *Macromolecules* **2002**, *35*, 6754−6756.
(33) Liu, J.; Sun, Y.; Deng, Y.; Zou, Y.; Li, C.; Guo, X.; Xiong, L.; Gao, Y.; Li, F.; Zhao, D. Highly Water−Dispersible Biocompatible Magnetite Particles with Low Cytotoxicity Stabilized by Citrate Groups. *Angew. Chem., Int. Ed.* **2009**, *48*, 5875−5879.
(34) Liu, D.; Li, Y.; Deng, J.; Yang, W. Synthesis and Characterization of Magnetic Fe_3O_4−Silica−Poly(γ−Benzyl−l−Glutamate) Composite Microspheres. *React. Funct. Polym.* **2011**, *71*, 1040−1044.
(35) Gonzato, C.; Courty, M.; Pasetto, P.; Haupt, K. Magnetic Molecularly Imprinted Polymer Nanocomposites via Surface−Initiated RAFT Polymerization. *Adv. Funct. Mater.* **2011**, *21*, 3947−3953.
(36) Gao, D.; Zhang, Z.; Wu, M.; Xie, C.; Guan, G.; Wang, D. A Surface Functional Monomer-Directing Strategy for Highly Dense Imprinting of TNT at Surface of Silica Nanoparticles. *J. Am. Chem. Soc.* **2007**, *129*, 7859−7866.
(37) Yan, H.; Qiao, F.; Row, K. H. Molecularly Imprinted-Matrix Solid-Phase Dispersion for Selective Extraction of Five Fluoroquinolones in Eggs and Tissue. *Anal. Chem.* **2007**, *79*, 8242−8248.
(38) Tan, C. J.; Tong, Y. W. Preparation of Superparamagnetic Ribonuclease A Surface-Imprinted Submicrometer Particles for Protein Recognition in Aqueous Media. *Anal. Chem.* **2007**, *79*, 299−306.
(39) Yu, B.; Zhang, X.; He, J.; Yang, K.; Zhao, C. Effect of the Template Molecules and Nonsolvent Additives on the Recognition Property of Molecular Imprinted Polyethersulfone Particles. *J. Appl. Polym. Sci.* **2008**, *108*, 3859−3866.
(40) Smet, D. D.; Monbaliu, S.; Dubruel, P.; Peteghem, C. V.; Schacht, E.; Saeger, S. D. Synthesis and Application of A T−2 Toxin Imprinted Polymer. *J. Chromatogr. A* **2010**, *1217*, 2879−2886.